

Twisting Instabilities of Stretched Elastomer Rods

A Summary of Experiments Performed

Tomás Gillanders

August 2023

Abstract

This document provides a summary of the work that I completed over the summers of 2022 and 2023 on behalf of Prof. Michel Destrade and Dr Giuseppe Zurlo. In these experiments, the deformations of stretched elastomer rods when subjected to torsion were considered. In this report, I outline the questions that were of interest to us, the actions that were taken, the complications that arose and how they were/were not overcome, the successes and shortcomings of the experiments, and advise on how I think one could build upon the work that I have done and the findings of this report.

Contents

1	Introduction	2
1.1	Acknowledgements	2
1.2	Aim of Experiments	2
1.3	Materials	3
2	Simple Tensile Tests	3
2.1	Apparatus & Method	3
2.2	Data Collected	4
2.3	Fitting the Neo-Hookean & Mooney-Rivlin Models	5
2.4	Complications that Arose	6
3	Axial-Torsion Tests	7
3.1	Remark on Axial-Torsion Tests	7
3.2	Apparatus	7
3.3	Measuring the Onset of Helical Instabilities	9
3.3.1	Preconditioning	9
3.3.2	Rod Slenderness	9
3.3.3	Amount of Twist	10
3.3.4	Torque	10
3.3.5	Development of Helical Structure	12
3.4	Successful Experiments	14
3.5	Shortcomings of the Experimental Setup	15
3.6	Suggestions for Further Experimentation	16

1 Introduction

1.1 Acknowledgements

The work described in this document was conducted over the course of the summers of 2022 and 2023 under the supervision of Prof. Michel Destrade and Dr Giuseppe Zurlo from the School of Mathematical and Statistical Sciences and with help from Dr William Ronan from the School of Engineering in University of Galway. I would also like to thank David Connolly and Juan Alberto Panadero Pérez for their help in providing training and access to the tensile testing machine that was used in performing the measurements that are described below. I would also like to thank my brother, Breandán Gillanders, for the advice and help he offered me with respect to producing the 3D printed components used in the final experimental setup and setting up the electronics and circuitry needed to drive the rotating clamp.

1.2 Aim of Experiments

These experiments aim to provide experimental justification of the work of Destrade and Zurlo, concerning their theoretical approach to describing the onset of elastic instabilities and continuous deformation of stretched elastomer rods under torsion as they transition from ‘straight’ configurations to ‘kinked/knotted’ configurations. This work builds on that of Gent and Hua who considered this phenomenon, but modelled/approximated the transition from straight to kinked configurations as occurring instantaneously.

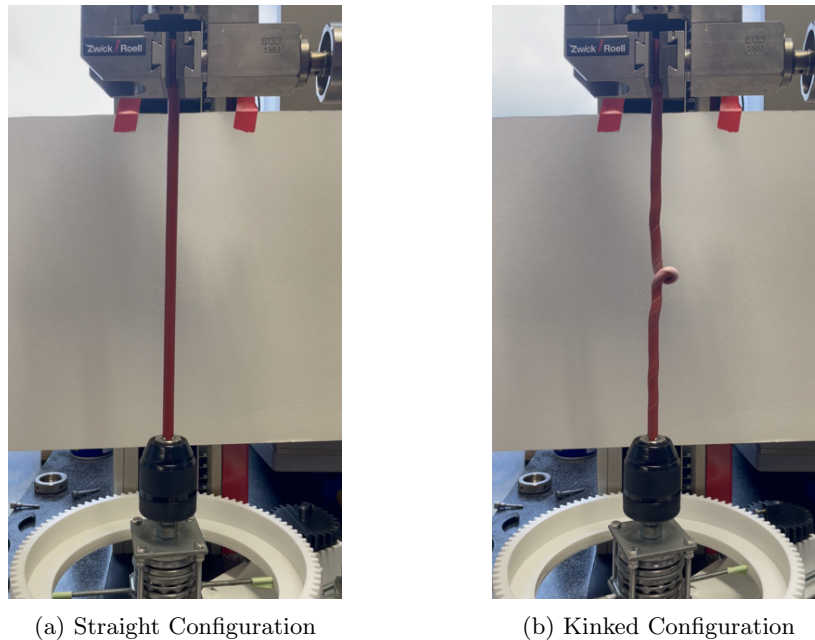


Figure 1

This instantaneous concentration of the “inherent elastic instability” at one point, as discussed by Gent and Hua, is a decent approximation for sufficiently large initial pre-stretches of slender rods. However, as will be demonstrated by the experiments described below, this analysis does not provide a complete description of the deformation of the rods in question.

In practice, it is observed that a different type of torsional instability initially occurs, in which the rod transitions ‘smoothly’ from a straight to a helical configuration; whose diameter and pitch develops as the rod is further twisted. Eventually, after sufficient twisting, the kink instability then takes over. It is this helical instability that is described by the work of Destrade and Zurlo and is of primary interest to this study.

In consultation with Zurlo, it was decided that the following questions were to be answered:

1. What value of torque (the *critical torque*, m^*) does the straight configuration of the rod disappear?
2. When the straight configuration disappears, is what appears a helix?
3. What happens to the helix as further torsion is applied? How do the diameter and pitch develop?
4. When is the deformation no longer *translation invariant*? (i.e. When does localisation of the instability begin to occur?)

In addition to the above questions, much of Gent and Hua’s experimental data was reproduced by Fionan O’Reilly under the supervision of Destrade. It was also an aim of the experiments described below to reproduce this data and to further develop/redesign the setup used by O’Reilly, as to improve the consistency of the data collected.

Unfortunately, due to circumstances outside of my control, time constraints and limitations to the equipment that was available for use, many of the above questions remained unanswered and the data that was of primary interest was not collected. However, throughout the process of designing the experiments, performing preliminary runs/checks on the equipment and failed measurements, much was learned about the complications that arose during the experimental process, possible solutions to these problems and how one might proceed to make the measurements that are described above.

1.3 Materials

The experiments were carried out on soft polyurethane rods (as seen in Figure 1). The rods had diameters ranging from 1mm to 8mm and were chosen as to resemble the materials used in the investigations of Gent and Hua and of O’Reilly as closely as possible.

Axial-Torsion measurements were also carried out using a bungee chord sample. Although this material is not considered in the analysis carried out by Destrade and Zurlo, it was found that the effects of interest are more pronounced, making the material suitable for demonstration.

2 Simple Tensile Tests

2.1 Apparatus & Method

Tensile tests were carried out using a Zwick Uniaxial Tensile Testing Machine equipped with either a 100N or 1kN load cell, depending on the tensile load ranges that were required for each

of the samples tested. Tensile force measurements were taken only during the loading phase.

The samples were tested up to strains between 20% and 50%, with the rods being extended at a rate of 100 mm/min.

The samples/rods were attached to the tensile testing machine using two different types of clamps in 2022 and 2023, as seen in Figure 2. We note that the clamps used in 2023 were more convenient to use since the grip-to-grip separation was independent of whether a material was clamped or not (Further discussed in Section 2.4).

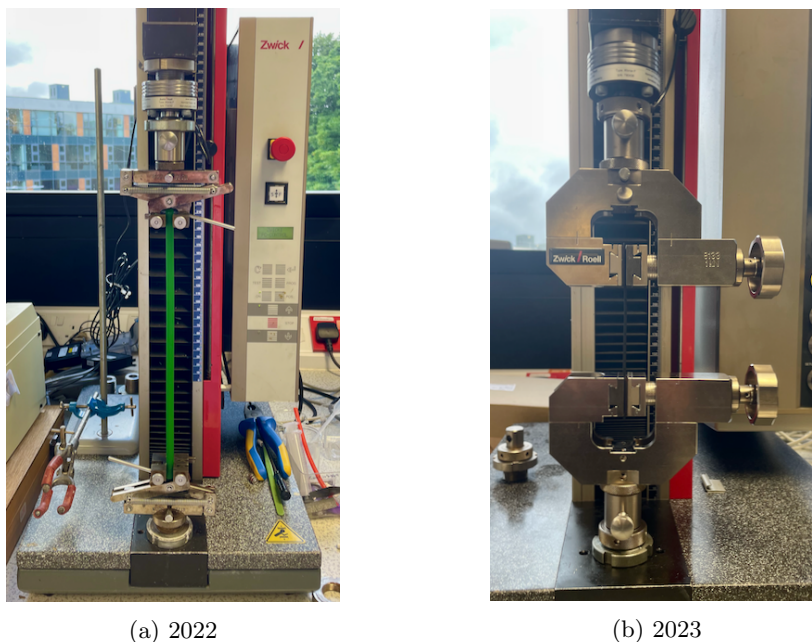


Figure 2: Tensile tester setup

2.2 Data Collected

The tensile measurements were made and recorded automatically by the Zwick Tensile Testing machine and accompanying software. In each case measurements of load and grip-to-grip separation (of the clamps) were of interest. For each material tested, multiple measurement runs were taken. It can be seen from these repeated measurements (Figure 3) that the elastic behaviour of the materials changed noticeably over the course of the first couple of runs. After approximately 5 conditioning runs, the elastic behaviour of the material was then observed to become reasonably consistent from run to run.

We note that in the stress-strain plots displayed in Figure 3, we have plotted the Cauchy Stress, σ , as a function of strain, λ . To determine the Cauchy Stress, the Nominal Stress, \mathcal{S} , was first determined by dividing the load by the cross-sectional reference area (as measured using a Vernier Calliper). To obtain the Cauchy Stress from this quantity, we then multiply the Nominal Stress by the stain:

$$\sigma_{11} = \lambda \mathcal{S}_{11} \tag{1}$$

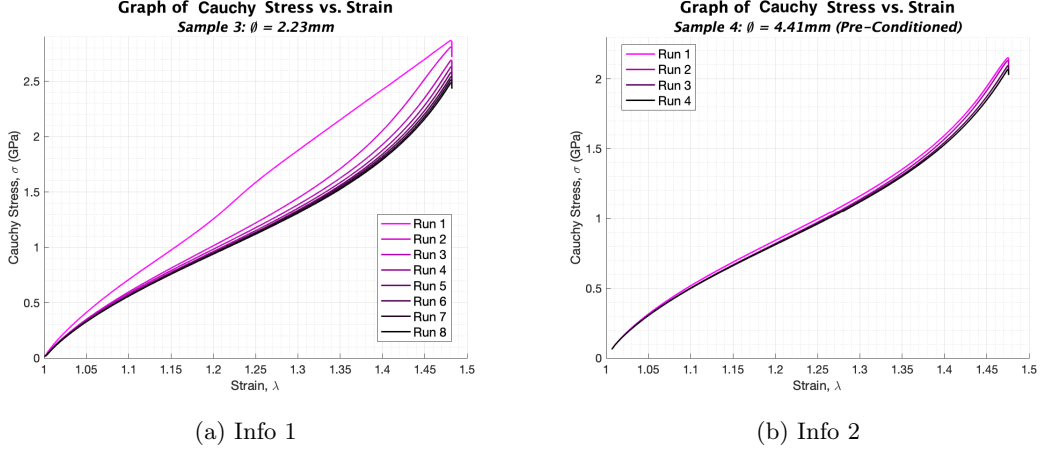


Figure 3: Samples of data collected for tensile test performed in 2023

where σ_{11} , S_{11} are the components of the respective stress tensors of interest.

2.3 Fitting the Neo-Hookean & Mooney-Rivlin Models

In determining the curve fittings, functionality from the Matlab ‘Curve Fitting Toolbox’ was used, allowing for the definition of custom models. The algorithms implemented by Matlab then determined the values of the parameters that provided the best fit to the data.

Fits using both the Neo-Hookean (Equation 2) and Mooney-Rivlin (Equation 3) elasticity models were performed, with stress-stretch relationships:

$$\sigma_{11} = \mu_0(\lambda^2 - \lambda^{-1}) \quad (2)$$

$$\sigma_{11} = C_1(\lambda^2 - \lambda^{-1}) + C_2(\lambda - \lambda^{-2}) \quad (3)$$

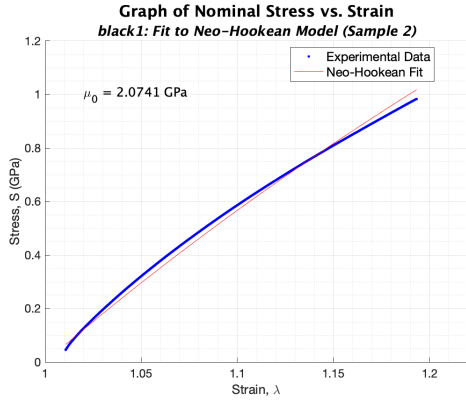
Note that for the data collected in 2022, it was the Nominal Stress, S_{11} , that was calculated and plotted, and not the Cauchy Stress, σ_{11} . The above equations had to be corrected to reflect this. The following equations were used for the fittings of the Neo-Hookean (Equation 4) and Mooney-Rivlin (Equation 5) models.

$$S_{11} = \frac{\sigma_{11}}{\lambda} = \frac{1}{\lambda} [\mu_0(\lambda^2 - \lambda^{-1})] \quad (4)$$

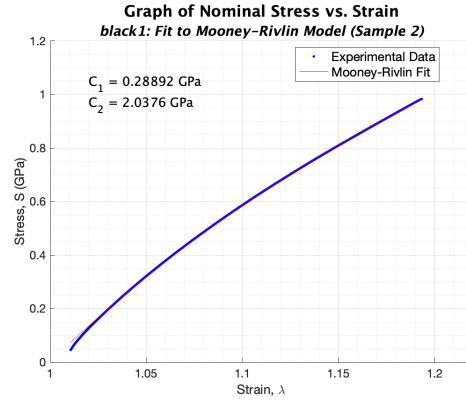
$$S_{11} = \frac{\sigma_{11}}{\lambda} = \frac{1}{\lambda} [C_1(\lambda^2 - \lambda^{-1}) + C_2(\lambda - \lambda^{-2})] \quad (5)$$

Matlab then determined the values of μ_0 , C_1 and C_2 that gave the best fits to the data.

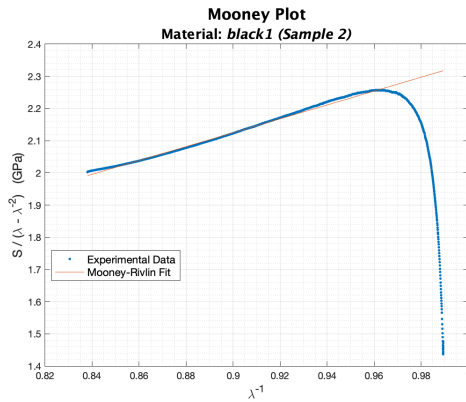
Examples of curve fitting performed on data collected in 2022 and 2023 are displayed in Figure 4. Figures 4a, 4b and 4c all correspond to the same sample from 2022, with Figure 4c being a Mooney Plot ($S_{11}/\lambda - \lambda^{-2}$ [or $\sigma_{11}/\lambda^2 - \lambda^{-1}$] against λ^{-1}), displaying the fit of the data to the Mooney-Rivlin model (that can be determined using a linear regression model).



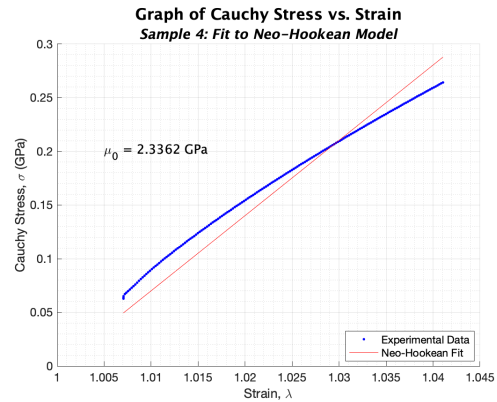
(a) Neo-Hookean Fit



(b) Mooney-Rivlin Fit



(c) Mooney Plot



(d) Neo-Hookean 2023

Figure 4: Curve fitting for collected for tensile test performed on a given sample in 2022 and another sample in 2023.

2.4 Complications that Arose

The tensile tests conducted on the materials were mostly routine and no major complications in the process were encountered.

The main complication arose from how the strain was measured and recorded by the Zwick Tensile Testing machine and TestExpertIII software. Strains were recorded by the software relative to the extension at which load measurements started to be recorded, and not the point at which the material was unstressed. All of the measurements are started at some specified amount of pre-load, as is the convention for tensile tests. Therefore, the reference length, L_0 , used by the software was incorrect. Therefore, in order to make sure that the correct strain measurements were being matched to the load measurements, the grip-to-grip separation recorded was used together with the pre-measured reference length of the material between the grips (when subject to no stress) were used to determine the strain.

It was also observed for the materials used that after pre-conditioning, some plastic deformation was always observed. It was therefore important to measure the reference length of the material

after the conditioning cycles, so that the correct strains were calculated.

3 Axial-Torsion Tests

3.1 Remark on Axial-Torsion Tests

Performing appropriately designed axial-torsion tests was of central importance to answering questions 1 through 4 as outlined in Section 1.2. Therefore, a great amount of thought and care was given when deciding how appropriate measurements should be made to answer the above questions, what apparatus should be used, and in the case where the ideal apparatus was not available, how should new equipment be designed and produced in order to alter the equipment that was available to perform the measurements needed.

3.2 Apparatus

The ideal apparatus required to perform the measurements of interest is an Axial-Torsion Machine, which is designed to impart both uniaxial tensile and torsional loads simultaneously to a sample and measure the material responses. However, the use of such a machine was not available during the period in which the experiments described were carried out. Therefore, the Zwick Uniaxial Tensile Testing machine, mentioned in Section 2.1, with modifications to the clamps was again used for the purposes of the axial-torsion measurements.

In order to twist the rod while under a tensile/axial load, a new clamp that attached to the testing bed/base of the tensile tester (see Figures 5b & 7a) was designed and created. The design of this clamp underwent a number of revisions in order to rectify issues that arose and to add features that allowed for the attempt of torque to be measured and, later on, for the clamp to be continuously twisted at a constant rate by a stepper motor.

The main body of the clamp is to be seen in Figure 5a and comprises of a drill chuck, two square washers, a circular washer, two thrust bearings, various nuts and bolts and some epoxy resin (only used to secure the bolt attached to the top plate so that the chuck would not twist when twisting the rod). Note also that the chuck was not fixed in place by the epoxy resin (so that it would be detachable). In order to make sure that the chuck did not unscrew itself while twisting, the rod was just twisted against the thread of the screw holding the chuck (However, it was found that for very slender rods, friction was enough to hold the chuck in place and thus, the direction in which the rod was twisted did not matter).

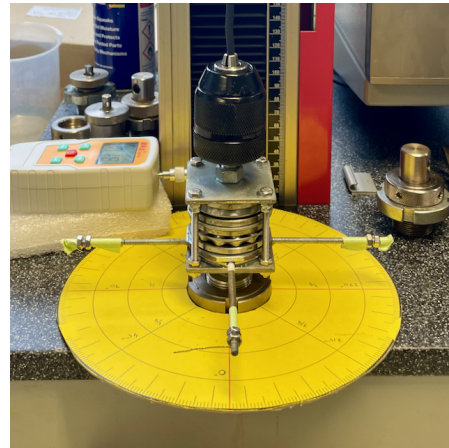
The construction of this first iteration of the clamp was cost effective (using only materials that could be purchased from any hardware store, although the thrust bearings were purchased online) and required only for some holes to be drilled into the corners of the square washers, so that that bolts holding the ‘top’ and ‘bottom’ sections of the clamp could be attached.

The second iteration of the twisting clamp design, as displayed in Figure 5b, incorporated metal rods that were fixed to the rotating portion of the clamp. These rods allowed for a force gauge to be used to determine the component of force, F_{\perp} , acting orthogonally to the rod, a known distance, d , from the axis of rotation of the rod. The moment of force or torque, M , could then be determined by the formula: $M = F_{\perp}d$. A length of wire was also wound around the end of one of these rods, and together with a graduated angle scale (the yellow scale shown in Figure 5b), allowed for the amount of twist applied to the rod to be measured.

The final iteration of the twisting clamp (Figure 5c) allowed for the rods being tested to be



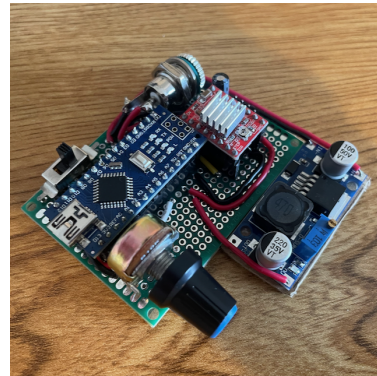
(a) First Iteration



(b) Second Iteration



(c) Third Iteration



(d) Circuitry and Electronics

Figure 5: Torsion clamp setup.

twisted at a constant, slow rate. This was accomplished by designing and 3D printing a pair of gears, one of which could be press-fit onto the bars of the clamp introduced in iteration 2, together with a stepper-motor driven by an Arduino Nano. The CAD files used for the gears and accompanying holder for the stepper motor, along with the Arduino code implemented can be found linked in Appendix A.

The circuitry required to drive the stepper motor is shown in Figure 5d, and a circuit schematic showing how the components are wired is displayed in Figure 6. The following is a list of the electronic components used:

- Arduino Nano
- NEMA 17 Stepper-Motor
- A4988 Stepper-Motor Driver
- LM2596 DC-DC Converter Module (Buck Converter)
- 10 k Ω Potentiometer

- SPST Switch
- 100 μF Capacitor
- 10 $\text{k}\Omega$ Resistor
- 12 V Power Supply (& jack)

The potentiometer and switch listed above allowed for the rate and direction, respectively, of rotation of the clamp to be adjusted, without having to recode the Arduino.

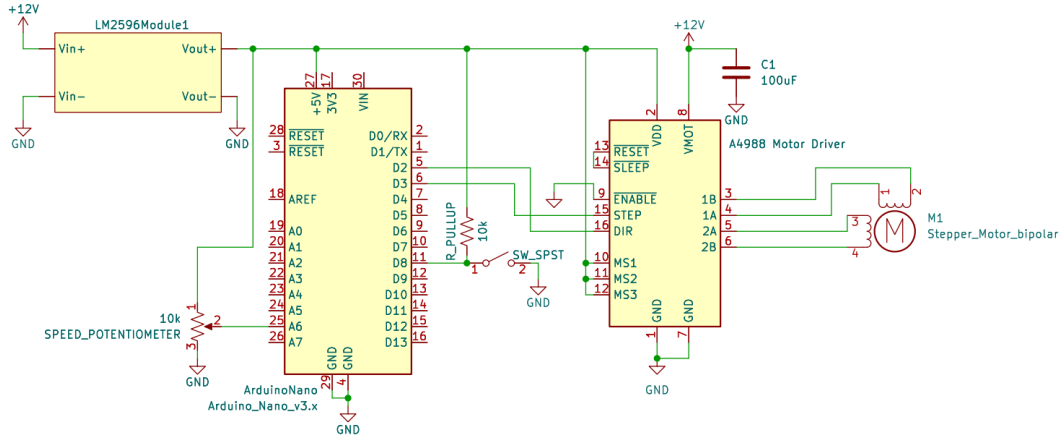


Figure 6: Circuit schematic for the electronics used to drive the torsion drive

3.3 Measuring the Onset of Helical Instabilities

A number of factors had to be considered when attempting to measure the onset of the suggested helical instability as discussed in Section 1.2. The following is a list of these main factors that were considered.

3.3.1 Preconditioning

As discussed in Section 2.2, preconditioning of the polyurethane rods was required such that the expected elastic behaviour of the rods be observed when performing the measurement runs.

For the axial-torsion measurements, both tensile (stretching) and rotational conditioning runs were performed. 5 stretching cycles were performed and two rotational cycles in each direction were performed before performing any measurement runs.

3.3.2 Rod Slenderness

The slenderness of the rods used in the experiments was a variable that was to be chosen such that the material response of interest was observed as clearly as possible. This choice of slenderness required experimentation with a variety of rods and in the case of the experiments described in this report, were determined purely subjectively. This was done due to time constraints associated with the project.

3.3.3 Amount of Twist

Measurements of the amount of twist applied to the rod were first obtained (when using the second iteration of the twisting clamp; see Section 3.2) by making measurements directly from the circular scale. As stated in Section 3.2:

A length of wire was also wound around the end of one of these rods, and together with a graduated angle scale (the yellow scale shown in Figure 5b), allowed for the amount of twist applied to the rod to be measured.

After introducing the stepper-motor driven twisting clamp, determining the angle of twist became slightly more difficult, and ultimately was not determined due to time constraints. The difficulty arose from the way in which the rotational speed of the clamp was determined, thus making the measurement of the amount of twist ‘difficult’. As mentioned in Section 3.2, a potentiometer was used to vary the rotational speed. This was convenient when performing the experiments, however, it meant that the rotational speed was not known without further measurement being made. In order to determine this rotational speed, a number of avenues could be explored.

- In place of using the potentiometer, simply code the Arduino to instruct the stepper motor to rotate at a known, pre-determined speed. This is in fact easier to do than implementing the variable speed using the potentiometer.
- Implement a rotary encoder or Hall effect sensor in the setup, which can then be used to measure the angle through which the clamp is twisted (as a function of time).
- Determine the rotational speed of the clamp directly from a video of the rod twisting. (i.e. one could determine from the video how long it takes, T for the clamp to make n rotations. The rotational speed, ω , of the clamp would then be

$$\omega = \frac{T}{2n\pi} \quad (\text{rad s}^{-1}) \quad (6)$$

- Some other clever method...

For the cases where the rotational speed, ω , of the clamp is determined, the angle of twist is obtained by simply multiplying ω by the time for which the clamp has been rotated from some the point of zero rotation. This can be determined from the time associated with a video of the rotating clamp.

3.3.4 Torque

Measuring torque happened to be one of the most difficult challenges that was encountered during the course of the project.

Figure 7 shows a first attempt of trying to measure the torque response of the rod as it was twisted. As discussed in Section 3.2:

The second iteration of the twisting clamp design, as displayed in Figure 5b, incorporated metal rods that were fixed to the rotating portion of the clamp. These rods allowed for a force gauge to be used to determine the component of force, F_{\perp} , acting orthogonally to the rod, a known distance, d , from the axis of rotation of the rod. The moment of force or torque, M , could then be determined by the formula: $M = F_{\perp}d$.



(a) Torque 1



(b) Torque 2

Figure 7: Setup for measuring torque using a force gauge.

A number of problems arose with this setup, making it unsuitable for use as a means of making the torque response measurements. The following are some of the problems that were observed to arise:

- For small values of torque (or force as measured by the force gauge), this setup proved to be very insensitive. This is the case due to the small amount of friction that is still present when the clamp is under an axial load, even though the thrust bearings are supposed to alleviate this friction and allow for free rotation. This insensitivity is especially unwanted when making measurements on very slender rods, making the measurements unusable.
- The strain relaxation of the rod when under tensile and torsional loads was very apparent when making the torque measurements. With every additional increment of twist of the rod, the torque was observed to decrease rapidly initially (as might be expected) and then settle to a more gentle decrease. However, the torque was not observed to settle, no matter how much time it was given between the twist increment and the torque measurement. In order to alleviate this effect, twist increments and torque measurements were made at pre-determined time increments; however, this attempted solution was not successful.

The relaxation behaviour of the material suggested that introducing discrete increments of twist to the material, with pauses between the twist, was not suitable for making the measurements of interest. This then led to the development of the continuously rotating clamp (last iteration of the clamp as discussed in Section 3.2) as seen in Figure 5c.

The use of the continuously rotating clamp then called for a method of making continuous measurements of the torque response of the material. Ultimately, all attempts to implement such a measurement system proved to be unsuccessful. The following possibilities were considered:

- Sourcing a torsional load cell that could be attached to the rotating clamp. This option proved to be very expensive when considering load cells suitable for measuring the range of torque that arose during the experiments.

- Using a simple DC motor to drive the rotation of the clamp at a *constant* rate and measuring the voltage applied across the motor and then comparing the voltage to a calibration curve of the motor for output torque as a function of voltage. This method was not feasible due to time constraints. To do this, one would have to wire a feedback loop; using a rotary encoder to determine the rate of rotation of the clamp, report this back to the Arduino, which would then have to adjust the voltage across the DC motor to keep it rotating at a constant rate. The constant rotation of the motor is vital for this method to work, so that the sum of the torques acting on the clamp (i.e. the motor acting on the clamp and the rod acting on the clamp) is always zero. This requires a knowledge of the electronics that would not have been possible to develop in the time-frame required.
- Using piezoelectric sensors together with flat, two-tooth prongs, as displayed in the sketch in Figure 8. Once again, time constraints did not allow for this method to be further developed. Deployment of this method would require a way to make readings from the piezoelectric sensors and calibration of these sensors, together with other obstacles that are bound to arise.

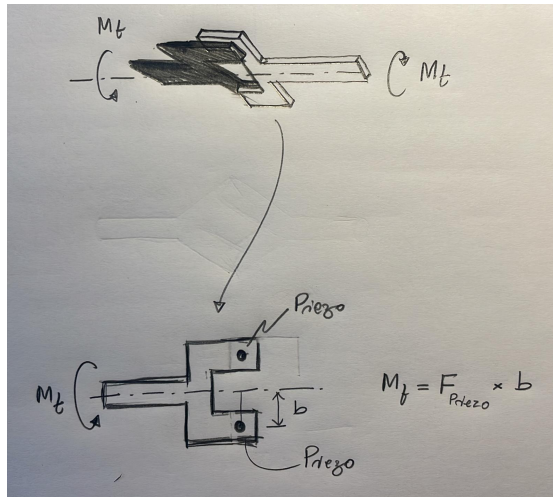


Figure 8: Diagram of proposed piezoelectric sensor-sensor based apparatus for measuring torque. Provided by Dr Giuseppe Zurlo.

3.3.5 Development of Helical Structure

The onset of the helical structure and its progression/development with increased twisting was one of the core question mentioned in Section 1.2. To reiterate what is required to be measured, we look for

1. the amount of torsion (the critical torsion) at which the straight configuration of the rod disappears,
2. is what appears a helix, and
3. how do the diameter and pitch of the helix develop with increased torque?

In order to answer the above questions, methods of image processing were explored. The high-level description of the intention of this image processing avenue is to take videos of the rod

samples as they are twisted and then using functionality provided by some image processing software package to analyse these videos; determining when transitions occur from one configuration of the rod to another, and measuring parameters such as the diameter and pitch of the helical structure that arises.

The setup used to accommodate this image analysis approach is shown in Figure 9. The setup is mostly the same as is described above, except for the inclusion of a line-laser that was directed along the length of the clamped rod and a checkerboard pattern that was placed ‘level’ with the rod, in the ‘plane of measurement’ (i.e. imagine that the rod were projected onto a flat plane, as it is the case when images/videos are taken of it). Of course, a camera placed on a tripod was also incorporated into the setup. For the purposes of this experiment a Canon digital SLR camera was used so that the camera parameters (e.g. zoom, focus, aperture, etc.) could be kept constant as the videos were taken. This was especially important since the camera calibration in the software used determined calibration parameters that were specific to the exact configuration of the camera used.

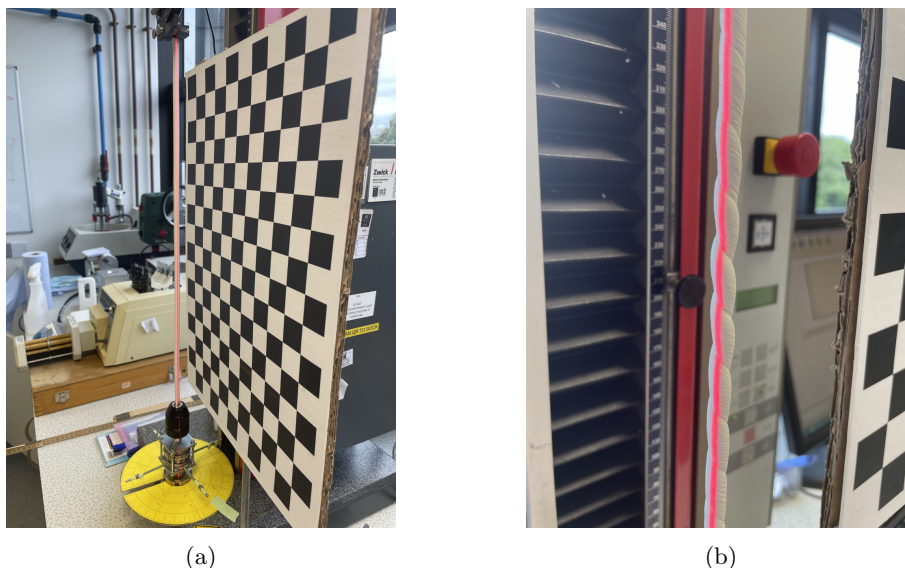


Figure 9: Setup for measuring properties of the helical deformation.

The purpose of the line laser used in the setup was to provide a high-contrast indication of the centreline of the rod in the videos, that then could be used to determine the rods deviation from a straight configuration.

To perform the frame-by-frame video analysis as described above, functionality provided by the MATLAB Image Processing And Computer Vision Toolbox was identified as a strong and intuitive to use candidate. Figure 10 displays an example of the output returned by the Camera Calibration Tool included with this software, when provided with 8 different images of the checkerboard pattern, taken from various angles. (Note that in practice, more calibration images should be used to obtain more accurate calibrations.)

Having determined these calibration parameters, the parameters can be exported and then used to undo the image distortion that arise due to the camera in the frames of the videos. Once this distortion is accounted for, the Image Processing And Computer Vision Toolbox software can

be used to make measurements of length directly from the images. When trialling this approach for making measurements of the rod samples, it was found that the length measurements made from the images were in surprisingly close correspondence with their true values. However, these were only subjective impressions and further experimentation would be required to quantify how good these measurements are.

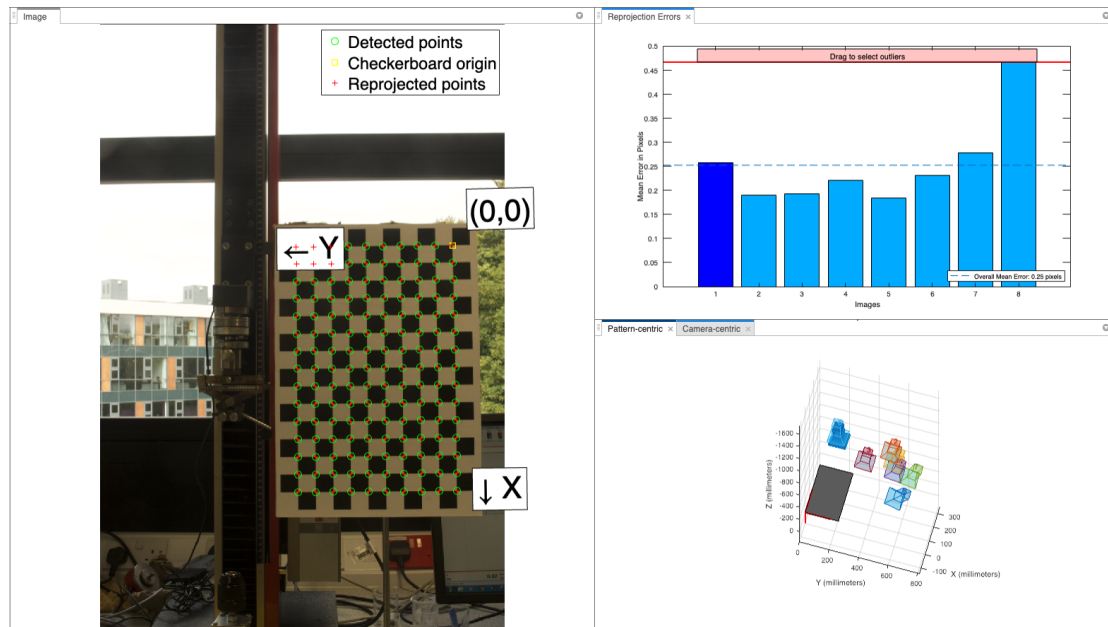


Figure 10: Image distortion calibration performed on a sample of 8 images using a checkerboard pattern and the MATLAB Image Processing And Computer Vision Toolbox.

3.4 Successful Experiments

While it was unfortunate that many of the quantitative measurements that were of interest in the context of this investigation into the onset of torsional instabilities of stretched elastomer rods, qualitative evidence of the helical deformations that are being described by Destrade and Zurlo was found and documented in the form of a series of videos.

The progression of deformation of one of the rod samples, as was captured in video, is displayed in the series of images seen in Figure 11. It is clearly seen from these images that, as the rod is twisted continuously as a slow rate, the rod does not simply transition from a straight to a kinked configuration, but passes through an intermediate helical configuration, as is predicted by Destrade and Zurlo. Furthermore, this helical configuration/deformation is first observed to be homogeneous in the material (i.e. translation invariant, away from the boundaries at least). After further twisting, the deformation is then observed to start localising in the material, which eventually culminates in the kink/knot that is described in the works of Gent and Hua.

Links to the videos taken of various rod samples are to be found in Appendix A.

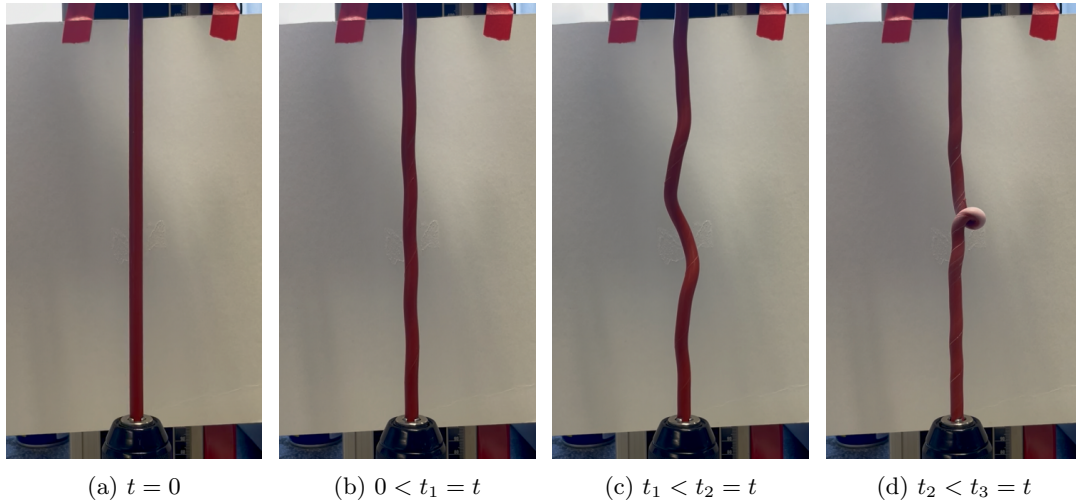


Figure 11: Progression of Deformation

3.5 Shortcomings of the Experimental Setup

The experimental setup as described in Sections 3.2 & 3.3 is far from ideal and gave rise to many issues that were ultimately not overcome over the course of the project.

The issue arising due to torque measurements, as discussed in detail in Section 3.3.4, was the greatest obstacle encountered. Torque measurements are of central importance when collecting data, as they provide quantitative measures that can be directly compared to the predictions of Destrade and Zullo. Without being able to measure this quantity, the collection of useful data was greatly hindered.

Another shortcoming of the experimental setup was the inefficiency when it came to making various measurements. Most of the methods devised for measuring various parameters, such as the static torque measurements, were extremely and unnecessarily time-consuming; resulting in time being spent poorly, manually making and recording the measurements, where it could have been better spent further developing the methods being used. However, it should be noted that it is also important at some stage during the development process to accept the setup will not be perfect and make measurements with the equipment on hand. Unfortunately, in the case of this project, the stage at which reliable and repeatable measurements could be made consistently was not reached.

The final point does not concern the experimental setup itself, but rather, the detection of the onset of the helical deformation as displayed in Figure 11b, and furthermore, when localisation of the stability (Figure 11c) begins to occur. Although the video analysis method, as discussed in Section 3.3.5, was developed such that these instances could be pinpointed, it was found (and is clear from the videos linked below; Appendix A) that the transitions between these different stages of deformation occur gradually and the effects are very subtle at first. This ultimately leads to large uncertainties in the data collected.

3.6 Suggestions for Further Experimentation

The following is a list of suggestions for how the experimental setup should be changed and what aspects of the experiment should be given thought if further experimentation were to be pursued.

- The most suitable setup for performing the measurements as described in this document would consist of an axial-torsion machine, with the tensile and torsional load cells rated for the suitable range of loads. All of the work carried out for setting up the measurements as discussed in Sections 3.2 & 3.3 was done as to imitate the functionality provided by such a machine. By using an axial-torsion machine (or by acquiring a torsion load cell add-on for a tensile machine), all torsional and tensile load measurements can be made concurrently, continuously and automatically, with the rate of rotation of the rod easily varied and logged by the equipment's software. Use of such a machine would also allow for conditioning runs to be automated, further reducing wasted time. The measurements returned by such a machine would also be far more reliable, accurate and precise than any measurements that would be made manually with the setup described above.
- A method for best determining the slenderness of rods being used (discussed in Section 3.3.2) for the experiments, using a more objective metric should be devised. Determining such a slenderness and implementing it across all experiments may be reflected in a greater accuracy and precision in the measurements made.
- Further consideration should be given to how one should determine when transitions between different stages of deformation of the rods occur, as is discussed in Section 3.5. Ideally, a more objective method of doing so should be devised, rather than the subjective method of simply eyeballing the videos and making an 'educated guess' of when exactly the transitions start to take place.

4 Conclusion

It is my hope that the information provided in the above document will be of help to anybody who would like to pursue similar experimentation, but do not know where or how to begin. I have outlined the complications that I was met with, some of the mistakes that I made and also the successes and shortcomings of the experimental setup that I ultimately designed and implemented.

While I have not succeeded in obtaining the results that I originally set out to get, I have learned a huge amount about the intricacies and difficulties that are associate with such experiments. I hope that something can be taken from my observations outlined above, and help somebody better equipped (and possibly more competent!) than me to build and improve on what I have done.

A Accompanying Material

As for now, instead of making the data collected for the project public, it can be found in the shared OneDrive folder that I have created for this project.